Applied Physics A (2020)126:883
https://doi.org/10.1007/s00339-020-04070-8

Applied Physics A
Materials Science & Processing

RAPID COMMUNICATIONS

Intrinsic open-circuit voltage and short-circuit current of ferroelectric photovoltaic effect

Qiong Wu[1,2] · Xin Wu[1,2] · Shifeng Zhao[1,2]

Received: 16 July 2020 / Accepted: 12 October 2020

Abstract
Photovoltaic effect of $BiFeO_3$ (BFO) films prepared by sol–gel method was investigated. Both *J*–*V* curves with different polarization under illuminated conditions and the *J*–*V* curves with different polarization under dark conditions are measured. On this basis, this work provides a law that characterizes the intrinsic open-circuit voltage and short-circuit current density of $BiFeO_3$ films by the differentials between illuminated and dark open-circuit voltage, as well as short-circuit current density. Furthermore, the components of open-circuit voltage are determined in detail. The practical conclusions show that it is accurate to use intrinsic open-circuit voltage and short-circuit current to reflect the strength of ferroelectric photovoltaic effect, not the values under illumination.

Keywords Ferroelectric photovoltaic effect · *J*–*V* curves · Open-circuit voltage · Short-circuit current density

1 Introduction

Ferroelectric photovoltaic effect (FPVE) has received extensive attention since its theoretic open-circuit voltage is free from the limitation of the bandgap, which is attributed to the fact that the mechanism of photovoltage is different from the traditional semiconductor p-n heterojunction [1, 2]. Many theories like domain wall theory, schottky-junction effect and depolarization field model have been put forward trying to explain the mechanism of FPVE. Importantly, all these theories are based on the viewpoint that FPVE is a bulk effect because photocurrent exists in the entire medium.

For such bulk photovoltaic effect, the formation of photocurrent mainly includes three processes. Firstly, a number of photogenerated exciton pairs are produced when the ferroelectric films are illuminated by the light with the photon energy higher than the bandgap of the ferroelectric films. Then, these photogenerated exciton pairs are separated to form carriers by depolarization electric field (E_{dp}) derived from the remanent polarization or built-in electric field (E_{bi}) derived from the schottky barrier [3]. Finally, carriers are collected on the electrodes. Thus, photocurrent is obtained. Therefore, *J*–*V* curves are usually measured on experiments to reflect the strength of FPVE. Generally, it is considered that the larger is the value of the illuminated open-circuit voltage (OCV_i) and illuminated short-circuit current (SSC_i), the better is the FEPV, and otherwise is opposite [4–6]. While the dark *J*–*V* curves of unpolarized samples was referred to characterize the illuminated open-circuit voltage and illuminated short-circuit current, even *J*–*V* curves under dark conditions sometime was ignored [7–10]. However, since the ferroelectric polarization has an influence on the illuminated *J*–*V* curves, it must also influence the dark *J*–*V* curves that represents the inherent properties of the electrode/ferroelectric/electrode heterostructure, which is also an important factor in exploring the mechanism of FEPV. In other words, it is not intrinsic to reflect the strength of FEPV only by OCV_i and SSC_i. Therefore, it is very necessary to investigate the intrinsic open-circuit voltage (OCV) and short-circuit current density (SSC).

Different from the previous characterization on strength of the ferroelectric photovoltaic effect, this work aims to reveal the intrinsic OCV and SSC by the differentials between the illuminated and dark open-circuit voltage, as well as short-circuit current density in *J*–*V* curves of $BiFeO_3$ films with different polarization voltage. Based on the fact

✉ Shifeng Zhao
zhsf@imu.edu.cn

1 Inner Mongolia Key Lab of Nanoscience and Nanotechnology, Inner Mongolia University, Hohhot 010021, China

2 School of Physical Science and Technology, Inner Mongolia University, Hohhot 010021, China

Published online: 22 October 2020

that the variation laws of dark open-circuit voltage (OCV_d) and short-circuit current density (SSC_d) are different from those of OCV_i and SSC_i when the polarization voltages are different, we put forward the intrinsic OCV and SSC of $BiFeO_3$ films that it is accurate to reflect the strength of ferroelectric photovoltaic effect.

2 Experimental

$BiFeO_3$ films were crystallized on Pt/Ti/SiO_2/Si(100) substrates at the annealing temperature of 510 °C under oxygen atmosphere by sol–gel method. The preparing process can refer our previous work [11]. Then, Au was sputtered as the circular top electrodes with diameter of 200 μm. Thus, a typical capacitor structure Au/$BiFeO_3$/Pt was obtained for electrical and photovoltaic measurement. The experimental setup for photovoltaic behaviors was self-designed [12]. Photovoltaic response measurements were performed on a Stanford phase-locked amplifier between 300 and 780 nm using a 500 W Xe bulb illumination. Polarization–electric field (*P–E*) hysteresis loop was measured at the frequency of 1 k Hz using a ferroelectric test systems produced by Radiant Technologies. The illuminated and dark *J–V* curves of films was characterized using a Keithley 2400 voltage source meter to obtain the open-circuit voltage and short-circuit current density. The illuminated area for the films is about 8 mm^2 to obtain accurate experimental data.

3 Results and discussion

X-ray diffraction of BFO films was measured and shown in Fig. 1a. The main diffraction peaks appear and there are no secondary phases. Such results show that the crystallization of BFO films is very good. Surface morphology and cross-sectional SEM image are shown in Fig. 1b. It can be seen that BFO films are very flat and dense and the thickness of films is about 500 nm. *P–E* hysteresis loop of $BiFeO_3$ films is shown in Fig. 1c. Good ferroelectric properties are obtained with remanent polarization (P_r) of 48 μC/cm^2, which lays a good foundation for ferroelectric

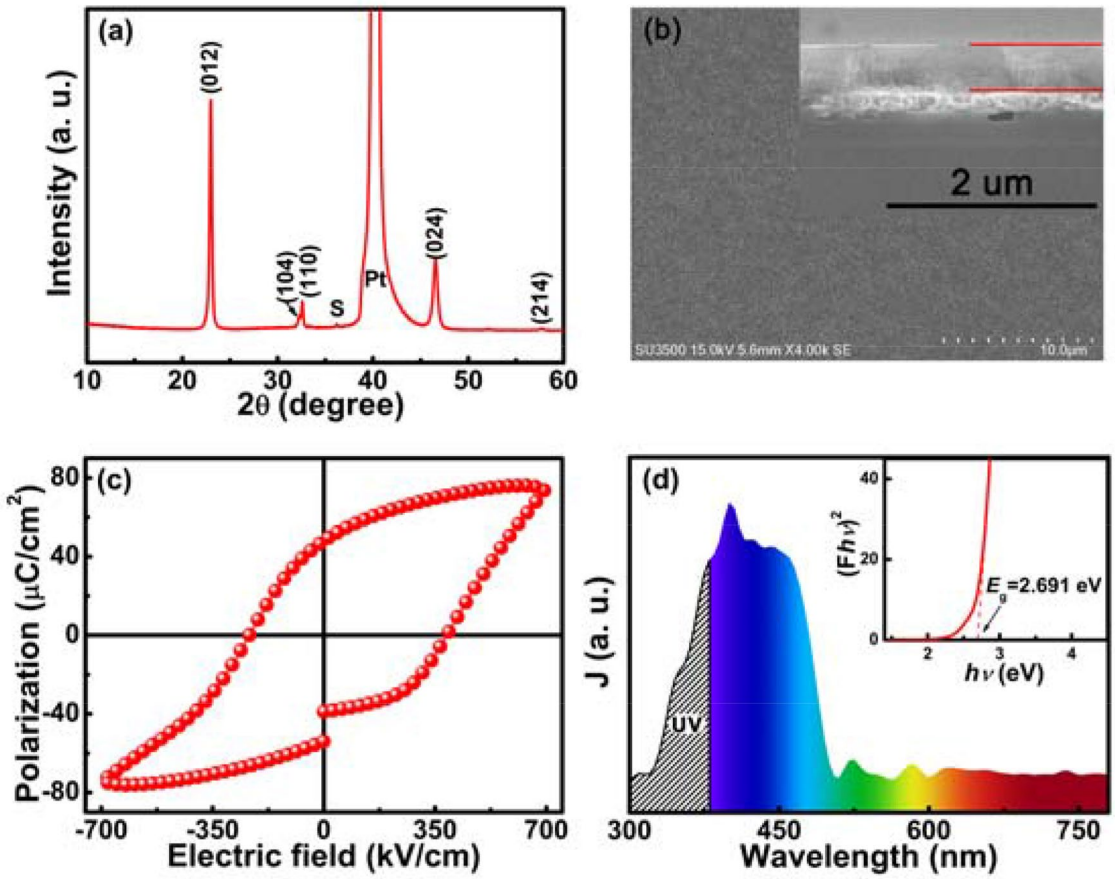

Fig. 1 **a** X-ray diffraction patterns of BFO films, 's' means substrate. **b** Surface morphology and cross-sectional SEM image of BFO films. **c** *P–E* hysteresis loop of BFO films, **d** spectral response from 300 to 780 nm for BFO films, the dotted area on the left represents the ultraviolet (UV) region, the inset is the bandgap calculated by reflectance spectra using Kubelka–Munk equation

photovoltaic effect. Notably, the coercive electric fields on the left and right sides are asymmetric with 230 kV/cm and 390 kV/cm, respectively, which means the schottky barriers at the upper and lower interfaces are different due to the difference between the top and bottom electrodes [13, 14]. In other words, the existence of E_{bi} leads to such asymmetric hysteresis loop.

Figure 1d presents photovoltaic response spectrum for BFO films. It presents a wide spectral response range in the near visible blue-violet region. Such spectral response is attributed to the narrower band-gap of BFO films. For accuracy, the bandgap of the BFO films is calculated by reflectance spectra using Kubelka–Munk equation [15]. As is shown in the inset of Fig. 1d, the bandgap derived from reflectance spectra is 2.691 eV, which is in good agreement with that of theoretical value. Meanwhile, the half-way point of the full width at half-maximum (HFWHM) is used to measure the central spectral response of the photocurrent. HFWHM of the photovoltaic response spectrum for BFO films is located at 420 nm, which shows a blue-shift compared with the theoretical wave 460 nm corresponding to the bandgap of 2.691 eV. Such blue-shift is originated from the fact that the surface-plasmon effect improves the absorption of visible light when Au is used as electrodes [16].

As mentioned above, E_{bi} and E_{dp} work together to separate photogenerated exciton pairs. Therefore, it is very important for the directions of E_{bi} and E_{dp} to confirm the motion law of carriers. It is not difficult to draw a conclusion that the direction of E_{dp} is opposite to the applied electric field. To determine the direction of E_{bi}, leakage current of $BiFeO_3$ films was measured, as shown in Fig. 2. It can be seen that it presents obvious asymmetric J–E curves when applied opposite electric fields, even, leakage current density with applied positive electric field is one order of magnitude higher than that with applied negative electric field, which indicates that it exists E_{bi} derived from the schottky barriers between the dielectric materials and the schottky barrier heights at the upper and bottom interfaces are different. The larger and fastly increasing leakage for the applied positive electric field shows that the direction of E_{bi} is as same as that of the positive electric field. That is to say, the direction of E_{bi} will not change with the direction of the applied electric field, always along the direction from bottom Pt to top Au electrodes.

It is suggested that the generation of E_{bi} is originated from the interactions of metal–semiconductor contacts between the dielectric films and electrodes since dielectrics can be regarded as wide bandgap semiconductors. Therefore, built-in electric field exits between Pt electrodes and BFO films, as well as Au electrons and BFO films. The direction of E_{bi} is determined by the carrier type of dielectrics and the differences for the work function between the metals and

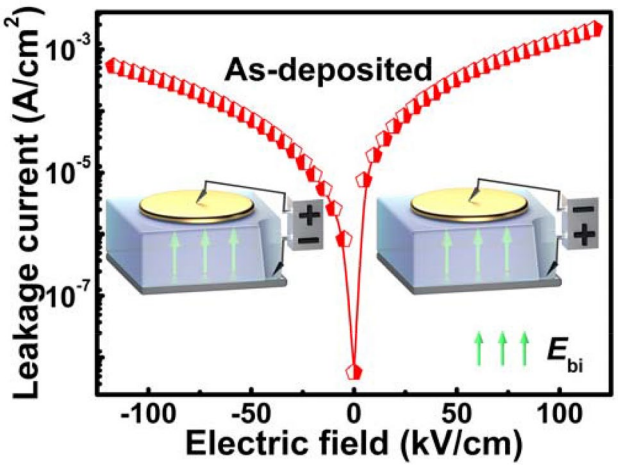

Fig. 2 Leakage current density–electric field curve, the inset on the right shows a positive electric field applied by the ferroelectric analyzer during leakage test, whereas the opposite electric field is shown on the left, the green arrow inside represents the direction of E_{bi}

semiconductors. To be specify, the schottky barrier heights are expressed by the equation,

$$V = V_D = (W_m - W_s)/q \quad (1)$$

where V_D is the schottky barrier height, W_m and W_s are the work functions of the metals and semiconductors, respectively. In this work, the work function of BFO films is considered to be ~ 4.7 eV, which is lower than those of Pt and Au electrodes with 5.65 eV and 5.1 eV, respectively [15, 17]. Therefore, the majority carries in BFO films are supposed to be p-type carries because the schottky barrier between Pt electrodes and BFO films is higher than that between Au electrodes and BFO films. While p-type carries are derived from the oxygen vacancies during the preparation [18]. Correspondingly, for metal–semiconductor contacts between the electrodes and BFO films, the energy bands of BFO films bend upward, forming a negative space charge region on the surface of BFO films, which results in the fact that the built-in electric field directs from the bottom electrodes to the films. Therefore, the direction of E_{bi} always directs from Pt to Au electrodes due to the differences of schottky barrier height.

To characterize the intrinsic open-circuit voltage and short-circuit current of the ferroelectric photovoltaic effect by excluding for the influence of E_{bi}, the positive depolarization field in the same direction as E_{bi} is built by applying negative polarized electric fields with polarization voltages of 3, 7 and 10 V, respectively. Figure 3a presents the dark J–V curves for the as-deposited and polarized $BiFeO_3$ films with different polarized voltage. It can be seen that the SSC_d value is between 0.2 and 0.4 μA/cm^2. And weaker SSC_d is observed due to the lower concentration carriers in the

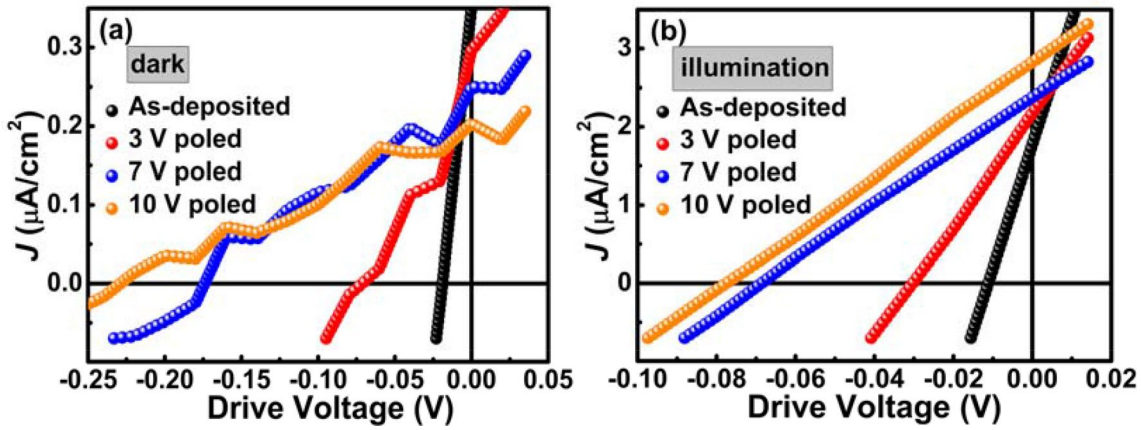

Fig. 3 *J–V* curves of $BiFeO_3$ films with different polarization voltage, **a** under dark conditions **b** under illumination conditions

dielectric films. However, OCV_d is comparatively higher. Interestingly, the values of OCV_d are 0.019, 0.071, 0.174 and 0.229 V with the applied polarization voltage of 0, 3, 7 and 10 V, respectively, which further indicates that the direction of E_{dp} is same as that of E_{bi}. While SSC_d gradually decreases with the increase of the polarization voltage, which presents the variation law different from OCV_d. Such results show that the concentration of the carriers decrease with the increase in the polarization voltage, which is ascribed to the conduction mechanic under dark condition. Under such conditions, the injected charges from the electrodes play a key role in the contribution to the carriers when applying the bias voltage [19]. While E_{dp} depresses the charge injection because its direction is different from that of the applied bias voltage. Therefore, the charge injected into the films will be less and less as the polarization voltage and E_{dp} increase.

Different from the properties under dark, *J–V* curves under illumination conditions are shown in Fig. 3b. Specifically, the current density under illumination conditions is higher one order magnitude than that under dark condition. This means that a large number of photogenerated exciton pairs are generated, which induces the higher photogenerated current. Moreover, the variation law of SSC_i is just opposite to that of SSC_d. That is to say, SSC_i increases with the increase of the polarization voltage, which presents the same variation law as OCV_i. Such results show the concentration of the photogenerated electron–hole pairs is much higher than that of the carriers injected from electrodes and photogenerated carriers play the more important key roles that injected from electrodes. Since it is supposed that the concentration of the photogenerated electron–hole pairs is nearly the same in all the films with different polarization voltage, the higher E_{dp} results in the higher photogenerated current. Therefore, SSC_i increases with the increase in the polarization voltage. Domain walls are considered to be one of the sources of ferroelectric photovoltaic effect [20]. The photovoltage in the monocrystal BFO films increases linearly with the total number of domain walls along direction of perpendicular to the domain walls. However, the film is polycrystalline in this work. Therefore, the domain arrangement is disorganized, which means the effect of domains on the results of this work is inconspicuous. The well-known issue of BFO is leakage current, which has a bad effect on the dielectric and ferroelectric properties of the films. To address this issues, a very low electric field of 10 kV/cm was applied during the measurement of the ferroelectric photovoltaic effect. Under so low electric field, the leakage current density of the films is about 10^{-8} A/cm^2 (Fig. 2), which is two orders of magnitude smaller than SSC_i. Therefore, the influence of leakage current on the ferroelectric photovoltaic effect can be ignored. Moreover, it is worth noting that there are some twists in the *J–V* curves under dark condition, which is attributed to the unstable electric transport behaviors since less carriers are more susceptible to be scattered by the potential field around the lattices. However, after illuminated, this simulation is improved and the electric transport becomes stable since the concentration of the carrier increases greatly. Based on the above discussion, SSC_i contains SCC_d that represents the inherent properties of ferroelectric films. Although the value of SCC_d is not worth mentioning compared with SSC_i, the differentials between SSC_i and SCC_d is the true intrinsic SSC. For intrinsic SSC, it would be $SSC_i - SCC_d$ rather than SSC_i.

Similar to SSC_i, OCV_i values are 0.011, 0.030, 0.068, 0.077 V with the increase of the polarization voltage. More interestingly, they are smaller than the values of OCV_d under the corresponding polarization conditions. Such results are originated from the intrinsic mechanisms for the ferroelectric photovoltaic effect. As shown in Fig. 4a, under dark conditions, only E_{dp} and E_{bi} contribute to OCV_d, which is determined by $E_{dp} + E_{bi}$ due to the same direction between them. After illuminated, a large number of photogenerated

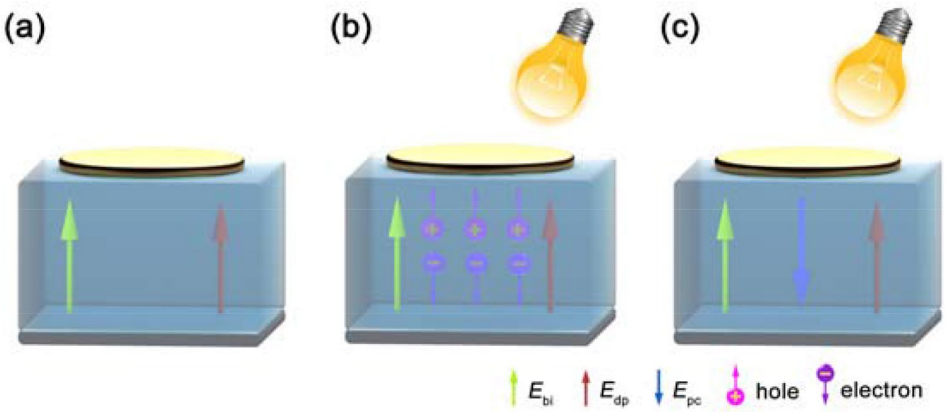

Fig. 4 **a** The depolarization field (red arrow) and the built-in electric field (yellow arrow) in the films under dark condition, **b** the segregation of the photogenerated carriers by driving from $E_{dp}+E_{bi}$ under illumination, **c** a negative electric field derived from photogenerated carriers (blue arrow)

exciton pairs are produced and separated by driving from $E_{dp}+E_{bi}$. Thus, the photogenerated electrons move towards to bottom Pt electrodes and the photogenerated holes move towards Au top electrodes because the direction of $E_{dp}+E_{bi}$ is positive, as shown in Fig. 4b. Hence, the bottom surface of the films is dominated by the electrons and the top surface of that is dominated by the holes. Therefore, a negative electric field derived from photogenerated carriers (E_{pc}) is built (Fig. 4c). In this case, the OCV_i measured on experiment is determined by $E_{dp}+E_{bi}-E_{pc}$, which explains why OCV_d is larger than OCV_i. Meanwhile, it is suggested that the value of E_{pc} is smaller than that of $E_{dp}+E_{bi}$. Based on the above discussion, it is inaccurate to reflect the strength of FEPV only by OCV_i. The intrinsic OCV of the FPVE would be OCV_d-OCV_i rather than OCV_i. In other words, the value of OCV is limited to $E_{dp}+E_{bi}$ rather band gap of materials.

To more clearly reflect the strength of intrinsic photovoltaic effect of $BiFeO_3$ films, the intrinsic VOC with the increase of the polarization voltage is compared with VOC_i as presented in Fig. 5a. It is shown that the intrinsic OCV of $BiFeO_3$ films is 0.008, 0.041, 0.106, 0.152 V for BFO films polarized by 0 V, 3 V, 7 V and 10 V, respectively. Compared with VOC_i, in the case of small polarization voltage, it is not much different from the intrinsic VOC. However, with the increase of the polarization voltage, the difference between VOC_i and the intrinsic VOC becomes more and more obvious. Such results indicate that E_{pc} grows faster than E_{dp}, which means that more photogenerated exciton pairs are separated. For ferroelectric photovoltaic effect, since open-circuit voltage reflects the ability that the ferroelectric films separate photogenerated exciton pairs, the intrinsic VOC is more accurate than VOC_i to reflect the ability to separate photogenerated exciton pairs for the ferroelectric films, especially at high polarization voltage.

Likewise, SCC under dark is also attributed to SSC under illumination. In other words, SSC_i are originated from the electric transport of the carriers including injected charges from the electrodes and photogenerated exciton pairs. Therefore, the intrinsic SSC derived from ferroelectric photovoltaic effect should be decided by SSC_i-SCC_d since it reflects the ability to produce photogenerated exciton pairs for ferroelectric films. Although the value of SCC_d is not worth mentioning compared with SSC_i, the differentials between SSC_i and SCC_d is the true intrinsic SSC. Figure 5b shows

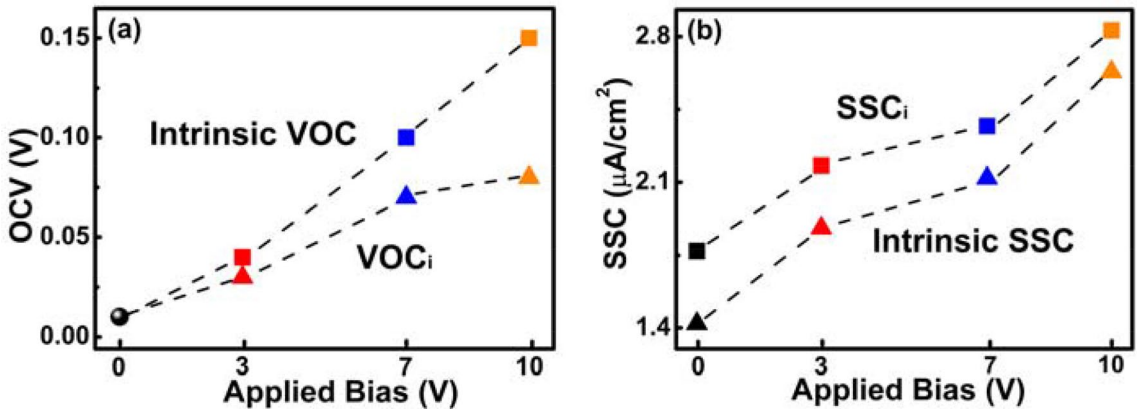

Fig. 5 The change of **a** intrinsic VOC and VOC_i and **b** intrinsic SSC and SSC_i with increasing applied bias

SSC and SSC_i curves with the increase of the polarization voltage. As can be seen, the intrinsic SSC values are 1.42, 1.88, 2.12, 2.63 μA/cm^2. In contract with the intrinsic VOC, difference between the intrinsic SSC and SSC_i gets smaller and smaller with the increase in the polarization voltage, which further confirms that charge injection is gradually suppressed with E_{dp} increasing.

In summary, the photovoltaic effect of $BiFeO_3$ films was investigated from the *J–V* curves under both illuminated and dark conditions with different polarization treatment. It is suggested that intrinsic VOC and SSC are determined by the differences between OCV_i and OCV_d, SSC_i and SSC_d, respectively. The intrinsic VOC and SSC are more accurate to characterize the strength of FPVE replacing OCV_i and SCC_i.

Acknowledgements This work was financially supported by the National Natural Science Foundation of China (Grant nos. 11864028, 12074204).

References

1. Y.Z. Sun, F. Guo, J.Y. Chen, S.F. Zhao, Appl. Phys. Lett. **111**, 253901 (2017)
2. S.Y. Yang, L.W. Martin, S.J. Byrnes, T.E. Conry, S.R. Basu, D. Paran, L. Reichertz, J. Ihlefeld, C. Adamo, A. Melville, Y.H. Chu, C.H. Yang, J.L. Musfeldt, D.G. Schlom, J.W. Ager, R. Ramesh, Appl. Phys. Lett. **95**, 062909 (2009)
3. F.G. Zheng, J. Xu, L. Fang, M.R. Shen, X.L. Wu, Appl. Phys. Lett. **93**, 172101 (2008)
4. R. Agarwal, Y. Sharma, R.S. Katiyar, Appl. Phys. Lett. **107**, 162904 (2015)
5. R.K. Katiyar, Y. Sharma, D. Barrionuevo, S. Kooriyattil, S.P. Pavunny, J.S. Young, G. Morell, B.R. Weiner, R.S. Katiyar, J.F. Scott, Appl. Phys. Lett. **106**, 082903 (2015)
6. R.K. Katiyar, P. Misra, F. Mendoza, G. Morell, R.S. Katiyar, Appl. Phys. Lett. **105**, 142902 (2014)
7. M. Qin, K. Yao, Y.C. Liang, Appl. Phys. Lett. **93**, 122904 (2008)
8. W. Ji, K. Yao, Y.C. Liang, Adv. Mater. **22**, 1763 (2010)
9. P.P. Biswas, S. Pal, V. Subramanian, P. Murugavel, Appl. Phys. Lett. **114**, 173901 (2019)
10. V. Batra, S. Kotru, J. Appl. Phys. **122**, 234101 (2017)
11. J.Y. Chen, W.Y. Xing, Q. Yun, W. Gao, C.H. Nie, S.F. Zhao, Mater. Lett. **11**, 601 (2015)
12. Y.L. Bai, J.Y. Chen, X. Wu, S.F. Zhao, J. Phys. Chem. C **120**, 24637 (2016)
13. K.V. Im, B.J. Kuh, S.O. Park, S.I. Lee, W.K. Choo, Jpn. J. Appl. Phys. **39**, 547 (2000)
14. J.J. Lee, S.B. Desu, Ferroelectr. Lett. Sect. **20**, 27 (1995)
15. H.B. Michaelson, J. Appl. Phys. **48**, 4729 (1977)
16. F.G. Zheng, P. Zhang, X.F. Wang, W. Huang, J.X. Zhang, M.R. Shen, W. Dong, L. Fang, Y.B. Bai, X.Q. Shen, H. Sun, J.H. Hao, Nanoscale **6**, 2915 (2014)
17. H. Yang, H.M. Luo, H. Wang, I.O. Usov, N.A. Suvorova, M. Jain, D.M. Feldmann, P.C. Dowden, R.F. DePaula, Q.X. Jia, Appl. Phys. Lett. **92**, 102113 (2008)
18. G. Geneste, C. Paillard, B. Dkhil, Phys. Rev. B. **99**, 024104 (2019)
19. Y. Zhou, X. Zou, L. You, R. Guo, Z.S. Lim, L. Chen, G. Yuan, J. Wang, Appl. Phys. Lett. **104**, 012903 (2014)
20. S.Y. Yang, J. Seidel, S.J. Byrnes, P. Shafer, C.H. Yang, M.D. Rossell, P. Yu, Y.H. Chu, J.F. Scott, J.W. Ager 3rd., L.W. Martin, R. Ramesh, Nat. Nanotechnol. **5**(2), 143 (2010)